

# Optical Delay Line Nanometer Level Pathlength Control Law Design For Space-Based Interferometry

Robert L. Grogan, Gary H. Blackwood, and Robert J. Calvet

Jet Propulsion Laboratory  
California Institute of Technology  
4800 Oak Grove Drive  
Pasadena, CA 91109

## ABSTRACT

The brassboard optical delay line was developed for the Interferometry Technology Program (ITP) at the Jet Propulsion Laboratory to support the space-based optical interferometry missions. This article is concerned with the discussion of control law design; implementation issues; and the quantification of closed loop performance results obtained in a laboratory experiment. Variations on the ODL brassboard design will be flown on the Space Interferometry Mission and New Millennium Separated Spacecraft Interferometer (or Deep Space 3). The described brassboard ODL was designed to meet not only the performance requirements for space interferometry but to also meet environmental requirements. The role of the ODL to equalize the pathlength between two collecting telescopes of an interferometer and a central beam combiner in order to detect and acquire white light fringes is discussed. Fringe visibility resolution requirements for space interferometry prescribe that the optical pathlength from the two collecting apertures must be equal and stable to within a few nanometers RMS. A control experiment was contrived to evaluate how well the brassboard optical delay line can control optical pathlength jitter. The classical frequency domain loop shaping techniques that were used to design compensators are examined. Included is a description of a methodology for managing the control authority for the three actuation stages, as well as, an input shaping technique for handling the large ( $1e9$ ) dynamic range issues. Experimental results characterizing closed loop performance control of residual optical jitter in an ambient laboratory environment are included.

Keywords: Optical, Delay Line, Control, Pathlength, Interferometry, Space Interferometry Mission, SIM

## 1.0 INTRODUCTION

Interferometry is the technology of combining the light from spatially distributed small collecting telescope apertures in order to synthesize the resolution of a single large aperture telescope with a diameter equal to the separation distance of the two smaller telescopes. The optical delay line (ODL) has a history of ground-based designs in use at the Mark III Interferometer at Mt. Wilson, Palomar Testbed Interferometer, and Navy Prototype Optical Interferometer. Illustrated in figure 1.1, the Space Interferometry Mission (SIM) design uses four interferometers mounted on a 10-meter long boom. Each interferometer collects light from two telescopes then passes the light down an optical train including passing through an optical delay line finally interfering the starlight from the collecting telescope pairs in a beam combiner. The optical delay line is used to adjust the path length between the two light collection points and the central beam combiner in order to equalize the two path lengths. The types of mechanical articulation required for space based interferometry optical pathlength compensation are long stroke quasi-static translation, slewing for compensating for the rotation of the spacecraft, and small amplitude and high frequency motion compensating for perturbations in optical pathlength induced by thermal distortions and spacecraft disturbances. The spacecraft motions are caused by the articulating and rotating components on the spacecraft propagating through the spacecraft structure.

Optical pathlength control is essential to obtain the astrometric measurements. As shown in the interferometer astrometric measurement illustration in figure 1.2, the light from a star arrives at one telescope sooner than the other resulting in an external optical path delay (OPD) given by  $x$  in the diagram. The external OPD is determined by introducing an internal OPD which exactly matches it. This is accomplished by controlling the optical delay line to inject internal optical path length in one arm of the interferometer such that fringes are observed. Feedback is used to adjust delay line position to remain at the peak of the fringe. An external metrology system measures the common interferometer baseline vector ( $\vec{B}$ , the distance between the corner cubes), and monitors minute changes in the baseline length. This measurement along with the fringe

position information ( $x$ ) is used to determine the angular separation between stars ( $\theta$ ) at the micro-arcsecond level via the following equation where  $\hat{s}$  is the unit vector orthogonal to the stellar wavefront:

$$x = \vec{B} \cdot \hat{s} = |\vec{B}| \cos \theta$$

Optical pathlength control requirements are driven by requirements on fringe visibility for astrometry and imaging as well as by the requirement for starlight nulling. The nulling requirement is the more stringent necessitating 1 nanometer RMS optical path difference (OPD) control over a broad frequency range. Fringe visibility requirements translate into the need for 10 nanometer RMS OPD control at frequencies above the fringe detector frame rate of approximately 1 kHz and more relaxed requirements at lower frequencies.

The purpose of the brassboard ODL hardware development was to mitigate technical risk, cost, and schedule early in the project development by performing design validation on selected components. The brassboard delay line component was designed to meet not only performance requirements, but also to meet environmental and reliability requirements anticipated for the interferometry missions. The brassboard design validation is intended to be limited in scope: critical design issues are to be rigorously addressed while avoiding the formality associated with full flight qualification that would normally occur much later in a flight mission lifetime. Although the brassboard ODL component is not destined to become either a flight or engineering model, the unit will nevertheless provide risk reduction and a firm set of recommendations to the project for any additional design, development, or qualification that are required. More details about the flight qualification tests and mechanical design of the brassboard ODL may be found in reference [1].

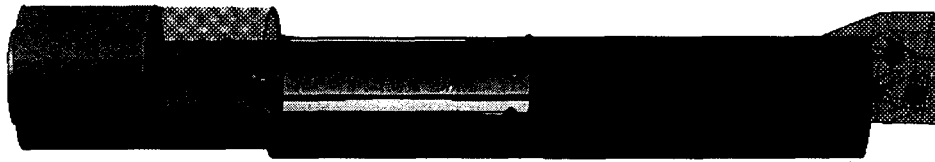


Figure 1.1: SIM Spacecraft Configuration

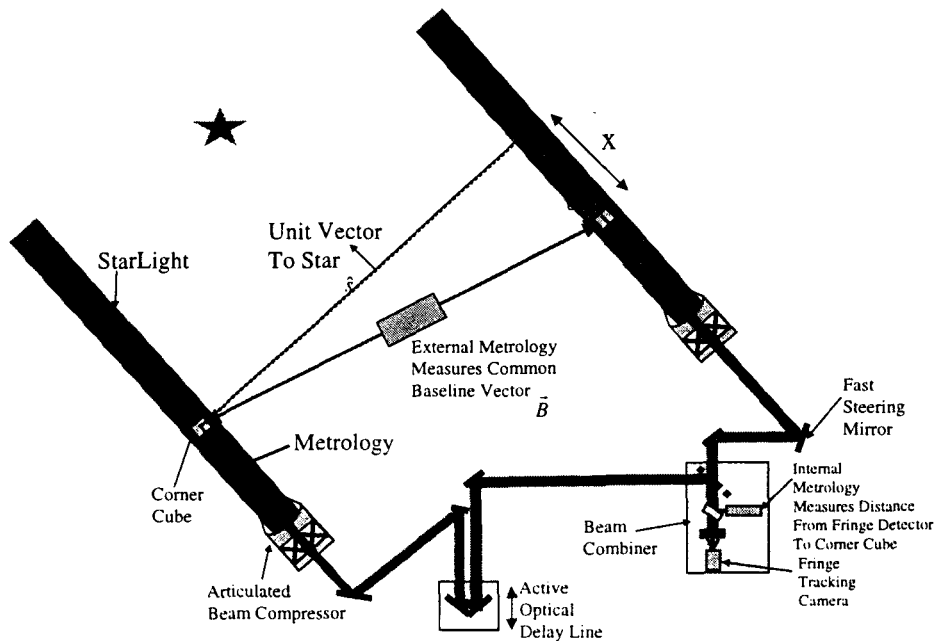


Figure 1.2: Illustration Of The Role Of ODL In SIM Astrometric Measurement Concept

## 2.0 MECHANISM DESIGN DESCRIPTION

The mechanical design philosophy for the optical delay line (ODL) was to create as many design concepts as possible that would allow a priori attainment of requirements, in order to minimize analysis, testing, and reliance on workmanship. Many of these concepts proved to be synergistic with each other attacking more than one requirement and creating a design robust to the operating environment. As a byproduct of this mechanical design philosophy all the areas of design that require refined or second order analysis and testing to validate or careful workmanship to insure success were attacked.

The brassboard ODL pictured in figure 2.1 was designed to take a 3 cm diameter collimated beam of visible starlight and coaxial metrology beams and pass it on to a beam combiner. Light enters the bottom aperture and exits the top (or vice-versa). The subset of functional requirements chosen for the ODL encompasses the SIM mission. Some of these requirements are simply specifications of required geometric size, optical figure of merit ( $\lambda/20$ ), and other mission parameters (beam diameter, overall stroke, surface accuracy, allowable defocus and de-center, slew and tracking rates); while others such as the actuator stroke lengths and bandwidths are derived requirements based on knowledge of disturbance environments and the desire to achieve good dynamic range overlap between actuation stages.

As illustrated in figure 2.2, the ODL is composed of three tiered actuation stages to accommodate the large dynamic range requirement (1 m stroke with  $<5$  nm stability). The coarse stage is a DC brushless motor, harmonic drive and band drive system that actuates a trolley on preloaded bearings at speeds up to 10 mm/sec. The second stage is a voice coil that actuates a cat's eye housing a primary mirror support on flexures with respect to the trolley over 3 mm. Finally, fine pathlength control is provided by a reactivated piezoelectric translator (PZT) mechanism beneath a 1.2 cm secondary mirror and operates over a range of 15 microns. The ODL is composed of mostly aluminum with Invar metering tubes. The base plate is fabricated as an aluminum honeycomb core sandwich, with rail supports and integral interface flexures. The ODL weighs about 13 kg. and has a peak power usage of 5 watts.

The brassboard ODL was designed to meet not only the performance requirements for space interferometry but to also meet environmental requirements. The brassboard ODL has survived random vibration (170 g peak acceleration), shock (1500 g of high frequency input), and thermal/vacuum (-20 degrees C to +60 degrees C for survival, +10 to +30 degrees C while operating in hard vacuum) testing. The design minimizes material contamination effects such as outgassing and also electromagnetic interference. The component was designed for a 5 year mission life and 3 years of ground life for a total of 8 years of design life and millions to hundreds of millions of operating cycles.

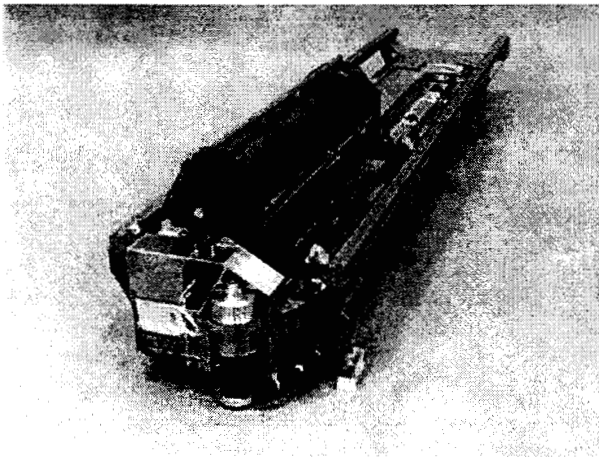


Figure 2.1: Optical Delay Line Brassboard Unit

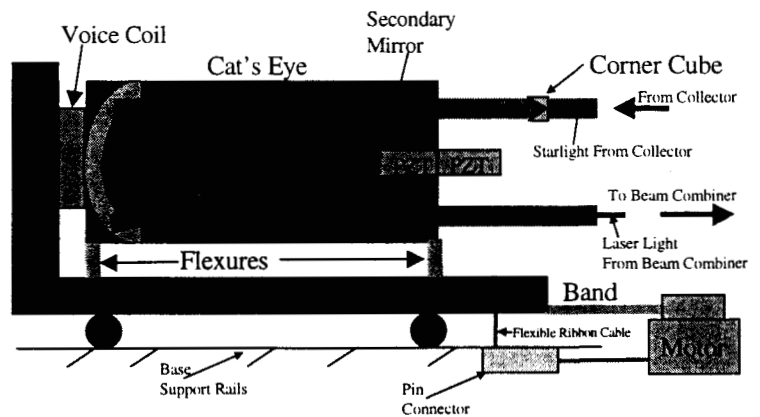


Figure 2.2: Optical Delay Line Diagram

## 3.0 EXPERIMENT DESIGN

An experiment was devised to evaluate how well the optical delay line could control optical pathlength jitter. Figure 3.1 provides the configuration for control experiment. All optical-mechanical components were mounted to a rigid optical bench mounted on compressed air isolation legs. The tool for the measurement is a 2 MHz heterodyne laser metrology system. The laser metrology system is an interferometer that acquires fringes by interfering a reference laser beam with a laser beam passing through the ODL optical path to a charge coupled device (CCD). The performance metric, as well as, the error signal for feedback control is the measured optical pathlength difference (OPD). The laser source is HeNe type with a wavelength of  $633e-9$  m. A digital phase meter counts phase difference between the reference and unknown with 8 bits of resolution

which is then passed to the real time computer (RTC) for processing. The digital counts are proportional to the OPD and are acquired at a rate of 5 kHz. The OPD is effectively the distance the laser light travels from the detector to the corner cube and back to the detector. Thus, by actuating the primary and secondary mirrors of the ODL in the direction of the incident laser light the OPD may be controlled. A unit change in mechanical position of the delay line approximately effects a four unit change in the OPD since the metrology laser beam passes through the component twice because of the corner cube retro-reflection. However, the optical jitter performance results shall be quoted in terms of one half of the total measured OPD since in the actual flight instrument starlight will traverse this path only once. Thus, in this sense the sensor has a resolution of 1.24 nm optical jitter.

The control laws were implemented digitally in two PowerPC processor cards housed in a VME card cage. Digital actuator commands are converted to the analog domain via two 16 bit digital-to-analog converter (DAC) cards for the PZT and voice coil actuators and via a custom board that converts a digital command in the RTC which commands a pulse train. The motor control unit accepts pulse train inputs from the specialized motor D/A card. The pulse train is then referenced to the pulses provided by the motor encoder. Thus, the rate of pulses generated is proportional to the commanded velocity of the motor stage. The motor has an additional internal encoder feedback loop that uses a PID type compensator with adjustable gains from a control unit interface/display embodied in a stand alone motor control unit.

Three nested synchronized multi-rate loop are used for the three control stages and operate at 100 Hz, 1000 Hz, and 5000 Hz for the motor, voice coil, and PZT stages, respectively. Code development and control design is accomplished on a workstation that communicates to the real time card cage by way of an Ethernet connection. More information regarding the software and electronics for this experiment can be found in references [2] and [3].

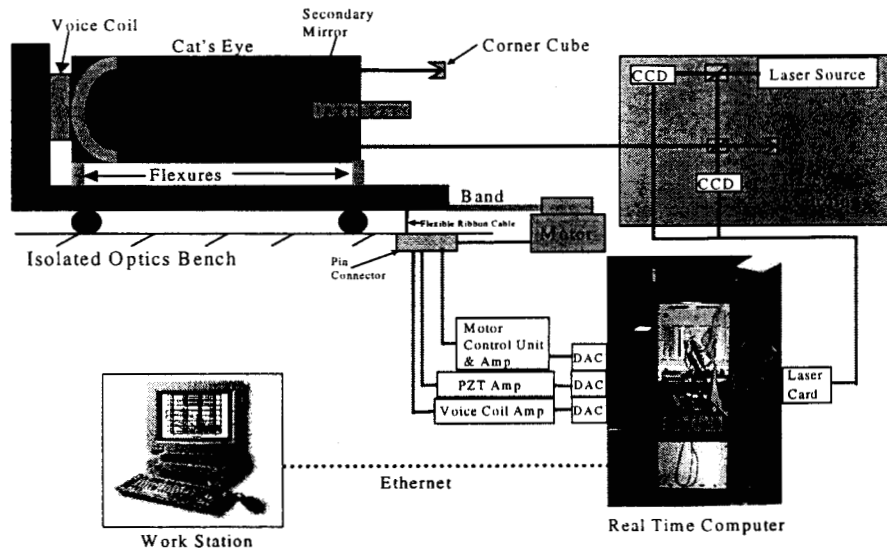


Figure 3.1: Experiment Setup

#### 4.0 PLANT DYNAMICS

Figures 4.1 and 4.2 display the voice coil and PZT transfer function data measured in the lab. Overlaid on these figures are the transfer functions of the parametric electro-mechanical dynamics model that has been developed in Matlab. A transfer function was additionally measured for the motor stage mechanical system, as well as, the control electronics (encoder feedback loop) integral with the motor unit.

The measured transfer functions include a zero order sample and hold due to the DAC and the computational pure time delay due to software processing in the RTC. To determine the time delay associated with sampling and computation the transfer function of the RTC was measured from a 16 bit Analog-to-Digital Converter (ADC) to each of the DAC's associated with the three command signals to the actuators. The phase of each transfer function was used to calculate the time delay. Accounting for the known rate of sample and hold (100 Hz motor, 1 kHz Voice Coil, and 5 kHz PZT) the computational pure time delay was found. The time delay model RTC was produced and put in series with the electro-mechanical dynamics model. The motor stage was additionally calibrated by inputting constant velocity digital commands and logging the resulting laser metrology measurement. The measurement was then scaled to mechanical position and slope information provided the attained velocity.

Several observations may be made from these plant transfer functions. The voice coil frequency response is flat at below the 3.5 Hz resonant mode of the flexure stage and thus actuates position at low frequencies. Above the resonant mode of the flexure stage the voice coil transfer function rolls off at 40 dB per decade and thus actuates acceleration. Complex conjugate poles of the resonant mode gives rise to a  $-180$  phase change at the eigen-frequency. Consequently, the flexure stage is open loop unstable above the resonant frequency (inverted pendulum) and phase lead will be required if the desired bandwidth is above the resonant frequency. The PZT actuates position up to 4 kHz and hence has a flat frequency response greater than the bandwidth of interest for control.

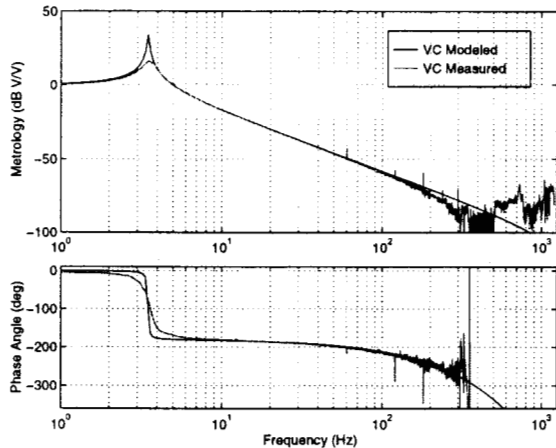


Figure 4.1: Voice Coil Plant Transfer Function

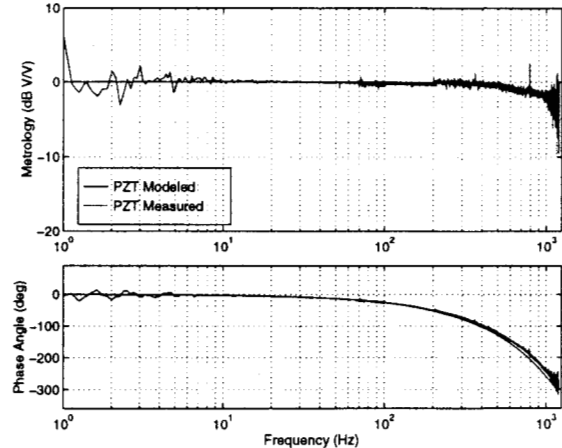


Figure 4.2: PZT Plant Transfer Function

## 5.0 CONTROL LAW DESIGN

The measured plant transfer functions were used to design compensators for the three control layers. Classical loop shaping techniques were used to design compensators by shaping the gain and phase of the open loop system in the frequency domain a single loop at a time. The reference or target signal to the closed loop system is a prescribed position to track. A feed-forward velocity command is used to prescribe the motor stage a desired constant velocity motion. The desired constant velocity is integrated in software to provide a position ramp for the closed loop to track. Figure 5.1 illustrates the block diagram for three input single output system.

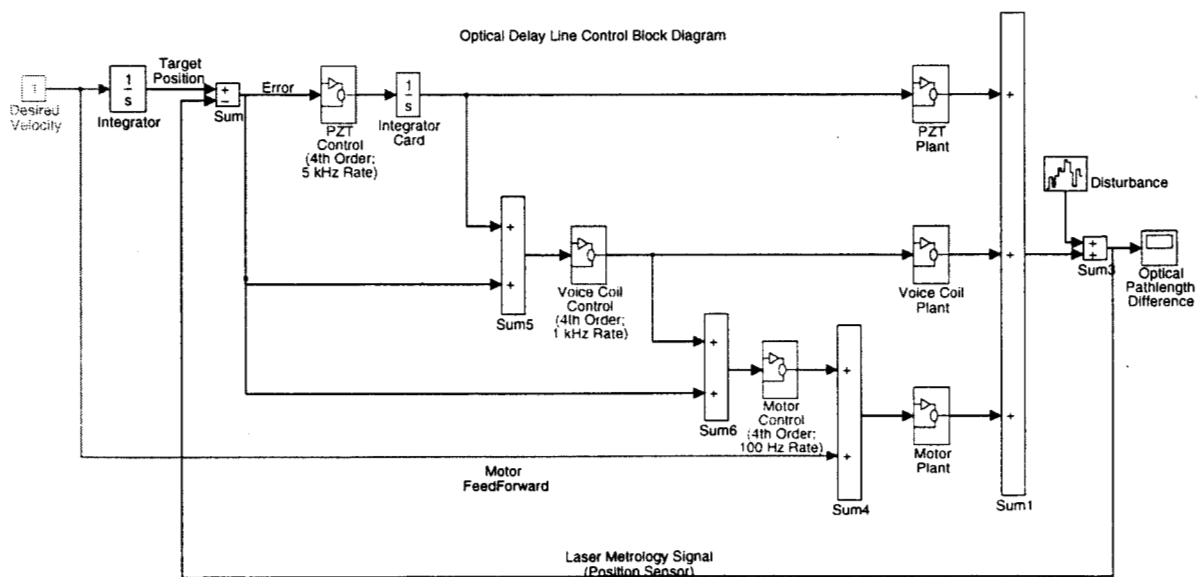


Figure 5.1: Control System Block Diagram

A cascaded compensator design methodology was used to design the control system. For this compensator structure the course stage (voice coil) desaturates and centers the fine stage (PZT) and similarly the motor stage centers the voice coil stage. The compensator of the fine stage drives the fine stage actuator as well as the input to the next stage compensator. This technique is used in previous delay line control designs at JPL (see references [4] and [5]). In this architect the inner loops are designed assuming outer loop controller is unity and plant has zero gain and phase response. In other words the inner coarse stage loop is designed assuming the outer fine stage loops are disconnected and feedback is obtained directly from the laser metrology sensor.

Figure 5.2 illustrates how the three nested loops are scaled. In the diagram  $G_p$ ,  $G_v$ , and  $G_m$  are the PZT, voice coil, and motor plants respectively. Similarly  $K_p$ ,  $K_v$ , and  $K_m$  are the compensators for the three loops. As shown the measured plants  $G$  are scaled by  $\gamma$  according to  $G'=G/\gamma$  such that  $|G'|=1$  at low frequency. The loop gains ( $K'G'$ ) of the scaled system shown in figure 5.3 are then shaped one at a time in the frequency domain. The total loop gain,  $L$ , of the scaled system is then given by:  $L'=K_p'(G_p'+K_v'(G_v'+K_m'G_m))$ .

Note that the total loop gain of the unscaled system is given by:  $L=K_p(G_p+K_v(G_v+K_mG_m))$  and is exactly equivalent to the scaled total loop gain, thus  $L=L'$ . In reference [5] it was observed that when the system is scaled in this manner that at the crossover frequency of the coarser stage loop the total loop gain is the product of the finer stage loop gain and the phase margin associated with the coarser stage loop gain. Below the crossover frequency of the coarse stage the total loop gain approximates the fine stage compensator in series with the coarse stage loop gain. Above the crossover frequency the total loop gain approximates the fine stage loop gain. Thus, this offers a convenient way to shape the loop gains in such a way that control authority handoffs and crossover frequencies are readily defined. As shown in figure 5.4, the PZT, voice coil, and total loop gain clearly illustrate the principal of the control authority handoff between the two stages at 20 Hz. The voice coil stage has control authority below 20 Hz and the PZT stage has authority above 20 Hz up to the total loop gain bandwidth frequency. This same strategy is also used to hand-off control authority for the voice coil to the motor stage at 0.1 Hz. Once the loops are shaped as desired the  $\gamma$  terms are accounted for in the designed compensators before implementation.

By convolving the measured open loop ambient disturbance power spectral density (PSD) with the square of the total loop sensitivity frequency response function  $S(j\omega)$  as shown in the below equation the appropriate amount of loop gain was determined. The predicted OPD variance was then utilized to find the loop gain required to achieve less than less than required RMS jitter across the frequency range within the bandwidth of control.

$$\Phi(\omega)_{\substack{\text{Closed Loop} \\ \text{Jitter} \\ \text{Predicted}}} = |S(j\omega)|^2 \Phi(\omega)_{\substack{\text{Open Loop} \\ \text{Jitter} \\ \text{Measured}}}$$

Additional signal paths were added to allow pass through of the low frequency sensor signal directly to each compensator due to high pass filters in the outer loop finer stage compensators. However the additional feed-through path do not effect loop hand off or crossover frequencies just the very low frequency loop gain. The final total loop gain of the system is then given by:  $L=K_p(G_p+K_v(G_v+K_mG_m))+K_vG_v+K_mG_m$ .

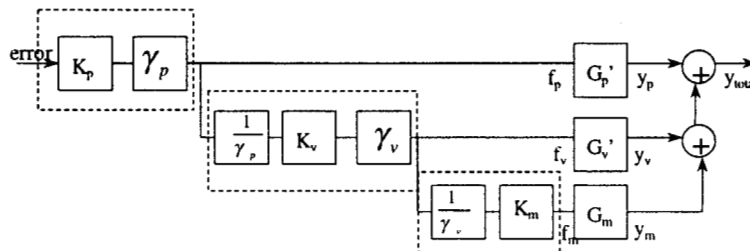


Figure 5.2: Cascade Control Architecture Scaling

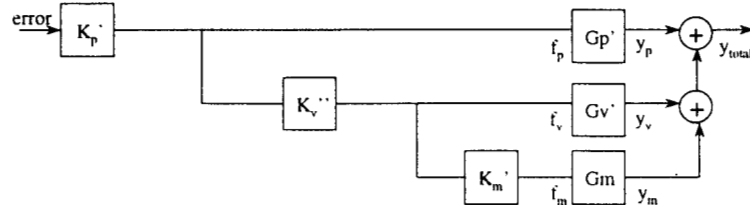
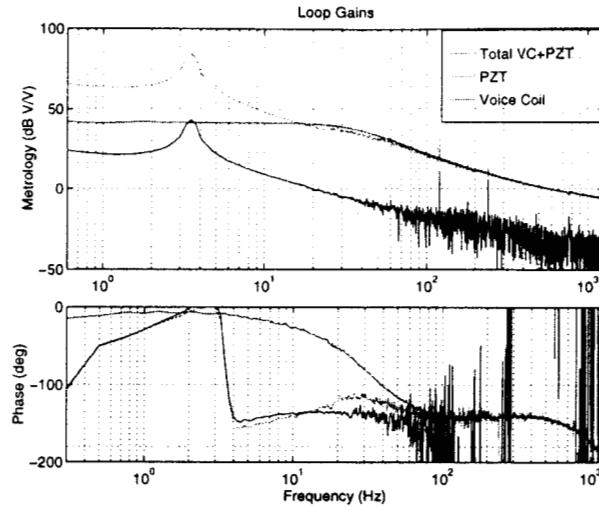


Figure 5.3: Cascade Control Design Architecture



**Figure 5.4:** Loop Gain Design

The compensator for the motor stage is composed of the following series of filters shown in the below equation: a gain, a narrow band notch filter at 3.5 Hz to prevent excitation of the voice coil stage flexure by the motor loop, and a low-pass filter at 6 Hz. The measured and predicted bandwidth, gain, and phase margin for the motor loop are contained in table 5.1.

$$K_{motor} = k_m \left( \frac{s^2 + 2k_n \zeta_n \omega_n s + \omega_n^2}{s^2 + 2\zeta_n \omega_n s + \omega_n^2} \right) \left( \frac{\omega_{lp}^2}{s^2 + 2\zeta_{lp} \omega_{lp} s + \omega_{lp}^2} \right)$$

(Notch) (Low Pass)

The compensator for the voice coil stage is composed of the following series of filters provided in the below equation: a gain, an integral lag at 3.5 Hz (integrates below 3.5 Hz) for low frequency disturbance rejection, a low-pass filter at 300 Hz, lead filter at 3.5 Hz provides phase stabilization at the low frequency flexure mode, lead filter at 70 Hz provides phase at crossover, and a high pass filter at corner frequency 0.1 Hz to prevent integration of DC signals. The voice coil compensator filters in series form a 8<sup>th</sup> order system. The frequency response of the discretized design voice coil compensator is practically indistinguishable from the measured as furnished in figure 5.6. Figure 5.7 shows the directly measured voice coil loop gain. The measured and predicted bandwidth, gain, and phase margin for the voice coil loop are contained in table 5.1.

$$K_{VoiceCoil} = k_v \left( \frac{s}{s + \omega_{hp}} \right) \left( \frac{s + \omega_{lag}}{s} \right) \left( \frac{\frac{s^2 + s}{a_1}}{\frac{s^2 + s}{b_1}} \right) \left( \frac{\frac{s^2 + s}{a_2}}{\frac{s^2 + s}{b_2}} \right) \left( \frac{\omega_{lp}^2}{s^2 + 2\zeta_{lp} \omega_{lp} s + \omega_{lp}^2} \right)$$

(High Pass) (Lag) (Lead) (Lead) (Low Pass)

The compensator for the PZT stage is composed of the following series of filters contained in the equation below: a gain, two integrators (one in hardware at the D/A and one in software), a lead filter at 900 Hz to provide phase at crossover, a lead filter at 1000 Hz to increase bandwidth and phase robustness, a high-pass filter at 0.1 Hz to prevent integration of DC signals, and a high-pass filter at 33 Hz to allow low frequency signals to pass through to the voice coil stage. The PZT compensator filters in series form a 9<sup>th</sup> order system. The frequency response of the discretized PZT compensator is practically indistinguishable from the measured as furnished in figure 5.8. Figure 5.9 shows the directly measured PZT loop gain. The measured and predicted bandwidth, gain, and phase margins for the PZT loop are contained in table 5.1.

$$K_{PZT} = k_p \left( \frac{1}{s^2} \right) \left( \frac{\frac{s^2 + s}{a_1}}{\frac{s^2 + s}{b_1}} \right) \left( \frac{\frac{s^2 + s}{a_2}}{\frac{s^2 + s}{b_2}} \right) \left( \frac{s}{s + \omega_{hp1}} \right) \left( \frac{s^2}{s^2 + 2\zeta_{hp} \omega_{hp2} + \omega_{hp2}^2} \right)$$

(Double Integral) (Lead) (Lead) (High Pass) (High Pass)

**Table 5.1: Control Analysis**

	<b>Gain Margin (dB)</b>	<b>Phase Margin (degrees)</b>	<b>Bandwidth (Hz)</b>
Motor Stage	50	100	0.1
Voice Coil Stage	15	45	20
PZT Stage	6	32	600
Total Loop	6	32	600

For each compensator the filters were connected in series and represented in state space form. Model order reduction was used to reduce each of the three compensators to 4<sup>th</sup> order state space systems. The state space model was transformed into modal tri-diagonal form and discretized via a bilinear (Tustin) approximation with frequency prewarping at the respective loop crossover frequencies. Zero terms were removed from discretized matrices and a Matlab script was written to automatically generate the C++ code to implement the discrete state space equations. The discretized equations are of the form:

$$x(k+1) = A \cdot x(k) + B \cdot u(k)$$

$$y(k) = C \cdot x(k) + D \cdot u(k)$$

Sinusoidal input shaping profiles given by the below equation were employed as compensator gain multipliers in the three loop stages to prevent actuator saturation resulting from the large dynamic range. Greater than 60 dB of total loop gain is required in order to provide the necessary disturbance rejection capability. However if the control is initialized at full gain large disturbance may saturate one or more actuators. This same strategy is used on the loop target velocity. At initialization all loop gains and the commanded constant velocity are zero. Full gain and command are achieved at 2 seconds. This method of ramping the loop gain up from zero requires infinite gain reduction margin to maintain stability or in other words the phase response of the total loop gain must not cross -180 degrees anywhere below the total loop crossover frequency.

$$a(t) = \left( 1 - \cos\left(\frac{2\pi t}{t_o}\right) \right)$$

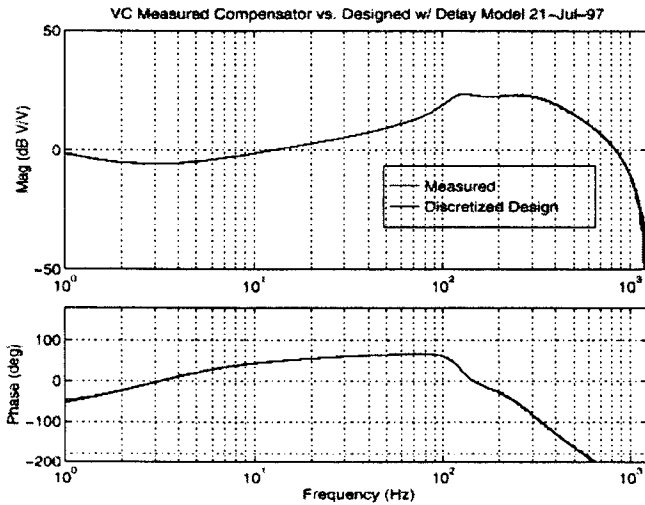


**Figure 5.6: Voice Coil Compensator Design**

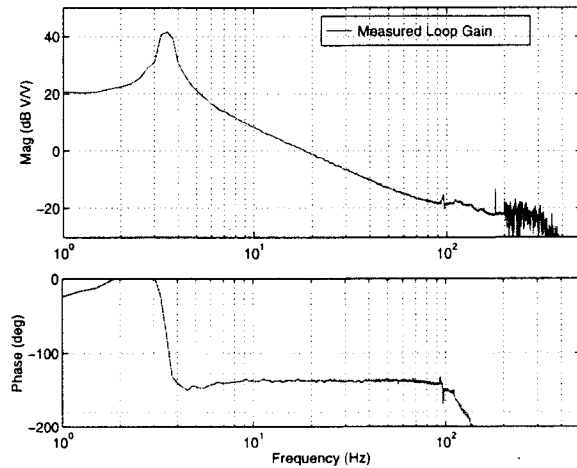


**Figure 5.7: Voice Coil Loop Gain**

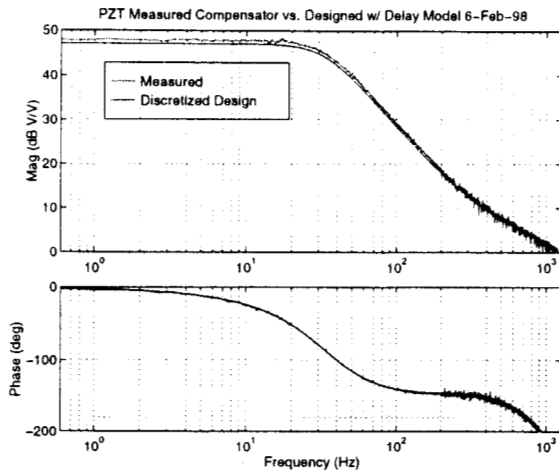


Figure 5.8: PZT Compensator Design

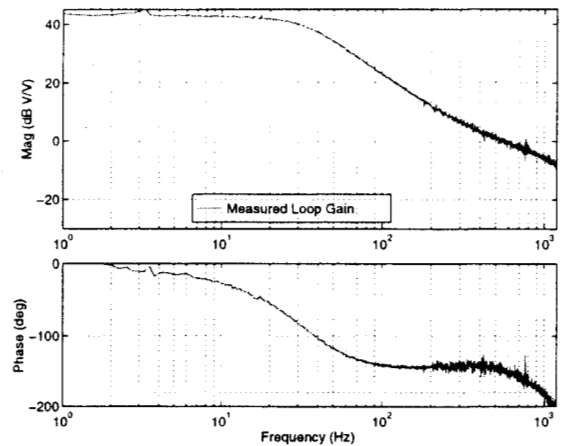


Figure 5.9: PZT Loop Gain

## 6.0 PERFORMANCE RESULTS ANALYSIS

Closed loop performance was measured to characterize two modes of operation. In the first mode of operation called tracking, the delay line is commanded to hold a stationary position and the capability to reject disturbance due to the ambient laboratory environment was measured to estimate the closed loop tracking performance. For the second mode of operation termed slewing, the delay line is command to articulate the trolley stage at 2 mm/sec constant velocity and the capability to reject disturbance due to both the ambient laboratory environment and self-induced disturbance due to motor stage motion was measured to estimate the closed loop slewing performance.

For both operating modes a 10 second time history of laser metrology signal data was acquired and converted to nanometers of optical jitter. The power spectral density (PSD) with units  $\text{nm}^2/\text{Hz}$  of the time signal was calculated. The open loop ambient and the total closed loop spectrums are shown in figure 6.1 for the stationary condition and in figure 6.2 for the 2 mm/sec slewing condition. Optical jitter is tabulated as the equivalent starlight OPD jitter (actual measured pathlength would be 2 times higher and in terms of mechanical jitter the results would be divided by a factor of 2). The residual RMS optical jitter was calculated for various frequency bins and is contained in table 6.1.

For the stationary case, 2.5 nm RMS residual optical jitter was recorded over the measured frequency range (up to 2.5 kHz). However within the bandwidth of control (600 Hz) less than 1 nm RMS residual optical jitter providing 44 dB of total attenuation was recorded within the bandwidth of control. Note the straight dashed line in figure 6.1 indicating the area above the bandwidth where the area under the PSD curve contains greater than the experimental goal of 1 nm RMS.

For the slewing condition, 5.4 nm RMS residual optical jitter was recorded over the measured frequency range (up to 2.5 kHz). However within the control bandwidth (600 Hz) 3.6 nm RMS residual optical jitter providing 85 dB of total attenuation was recorded within the bandwidth of control. Note the straight dashed line in figure 6.2 indicating the area above the bandwidth where the area under the PSD curve contains greater than the experimental goal of 5 nm RMS.

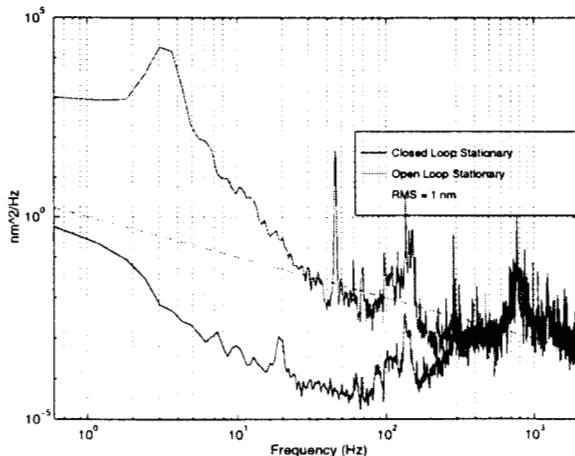


Figure 6.1: Residual Optical Jitter Stationary Condition

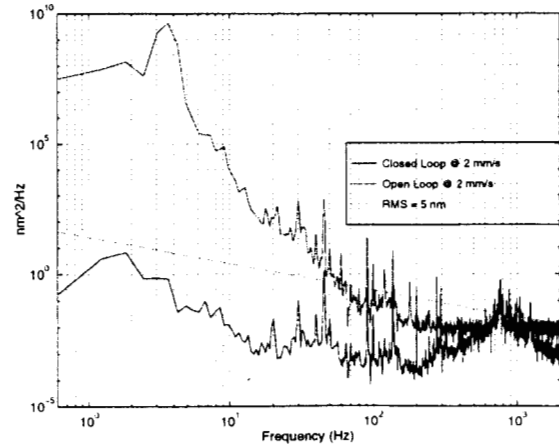


Figure 6.2: Residual Optical Jitter 2 mm/sec Slew Condition

**Table 6.1: Performance Results - Residual RMS Optical Jitter**

<b>Freq. Range (Hz)</b>	<b>RMS Jitter Open Loop Stationary (nm)</b>	<b>RMS Jitter Closed Loop Stationary (nm)</b>	<b>RMS Jitter Open Loop 2 mm/s (nm)</b>	<b>RMS Jitter Closed Loop 2 mm/s (nm)</b>
0 - 1	20.2	0.5	4374	0.3
1 - 10	159.5	0.4	65826	2.6
10 - 100	8.2	0.1	107.2	1.4
100 - 600	3.2	0.9	4.8	1.6
600 - 2500	3.3	2.3	3.2	4.1
0 - 2500	161.6	2.5	66075	5.4
0 - 600 (BW)	161.5	1.0	66075	3.6

## 7.0 SUMMARY

The brassboard optical delay line developed to support the space-based optical interferometry missions was utilized to demonstrate the feasibility of nanometer level optical pathlength jitter closed loop performance in the laboratory environment. A control law has been designed for the three stage single output system using classical loop shaping control theory. A methodology for managing the control authority of each actuator stage was shown, as well as, an input shaping technique for handling the large ( $1e9$ ) dynamic range issues. Closed loop performance testing experiments indicate that one nanometer performance is achievable within the control bandwidth of 600 Hz for the stationary operating condition. At issue is the fact that the performance measurement was taken in the loop, that is, the sensor used for performance measurement was used as the control feedback sensor. Ultimately, the performance measurement will be white (star) light fringe visibility. The functionality to acquire and closed loop track white light fringes is presently being implemented in the interferometry lab at JPL.

## 8.0 ACKNOWLEDGEMENTS

The work described in this paper was carried out at the Jet Propulsion Laboratory, California Institute of Technology, under contract with the National Aeronautics and Space Administration.

## 9.0 REFERENCES

- [1] Calvet, R., Joffe, B., Moore, D., Grogan, R., Blackwood, G., "Enabling Design Concepts for a Flight-Qualifiable Optical Delay Line," Proceedings of the 1998 SPIE Astronomical Interferometry Conference, Vol. 3350.
- [2] Johnson, R., McKenney, E., Slye, D., Starr, K., "Real Time Control Software For Optical Interferometers: The RICST Testbed," Proceedings of the 1998 SPIE Astronomical Interferometry Conference, Vol. 3350.
- [3] Irwin, P., Goullioud, R., "Hardware Design and Object-Oriented Hardware Driver Design For The Real Time Interferometer Control Systems Testbed," Proceedings of the 1998 SPIE Astronomical Interferometry Conference, Vol. 3350.
- [4] Colavita, M., Hines, B., Shao, M., Klose, G., Gibson, B., "Prototype High Speed Optical Delay Line for Stellar Interferometry," SPIE International Symposium on Optical Applied Science and Engineering, July 1991.
- [5] Spanos, J., Rahman, Z., "Optical Pathlength Control on the JPL Phase B Interferometer Testbed," Fifth Annual NASA/DoD Control Structure Interaction Conference, March 1992.

**JPL**

Present at SPIE conference on Astronomical Interferometry  
on 3/20/98, Kona, Hawaii

# Optical Delay Line: Nanometer Level Pathlength Control Law Design For Space-Based Interferometry

Robert L. Grogan, robert.grogan@jpl.nasa.gov

Gary H. Blackwood, gary.blackwood@jpl.nasa.gov

Robert J. Calvet, rcalvet@pop.jpl.nasa.gov

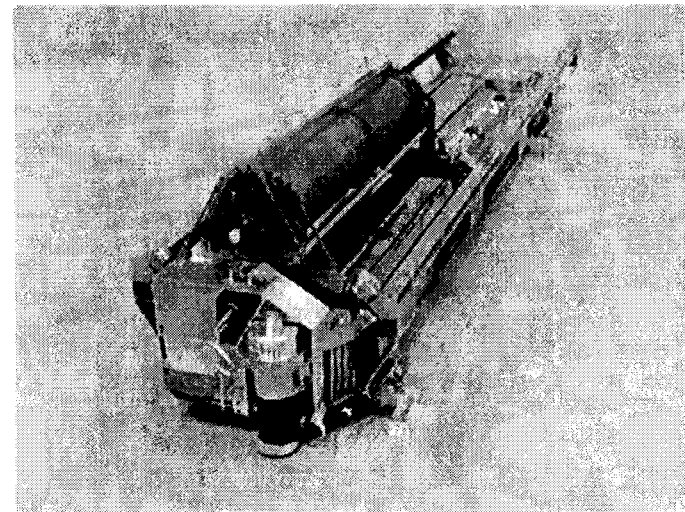
Space Interferometry Mission

Interferometry Technology Program

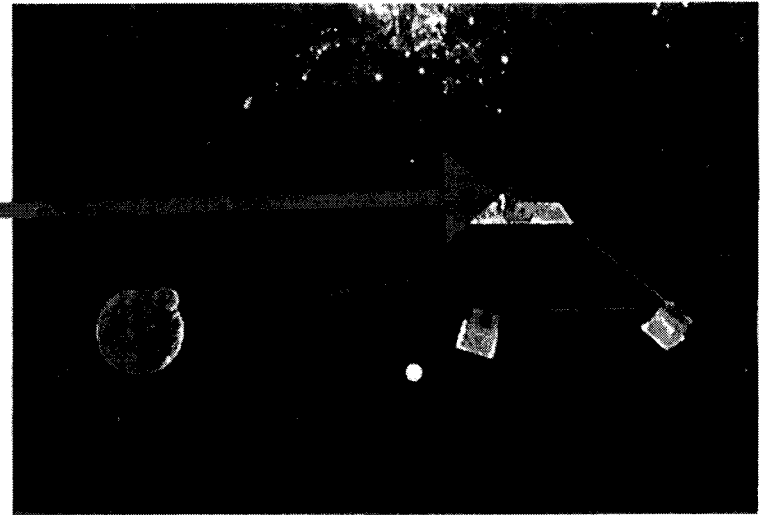
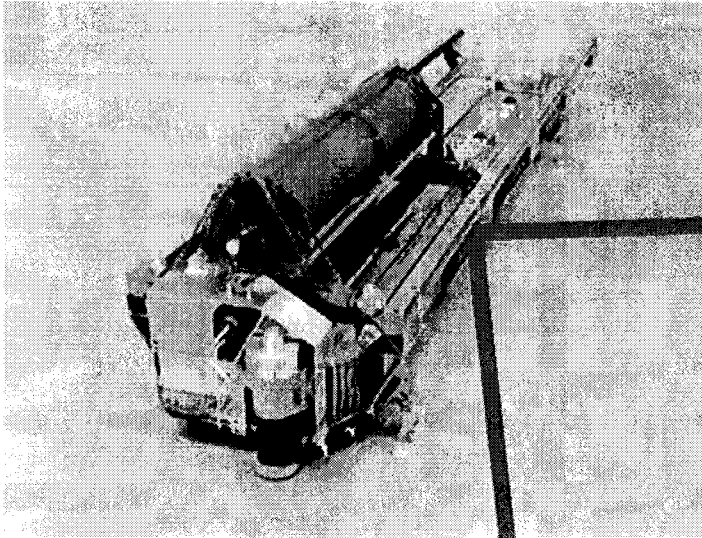
Jet Propulsion Laboratory

California Institute of Technology

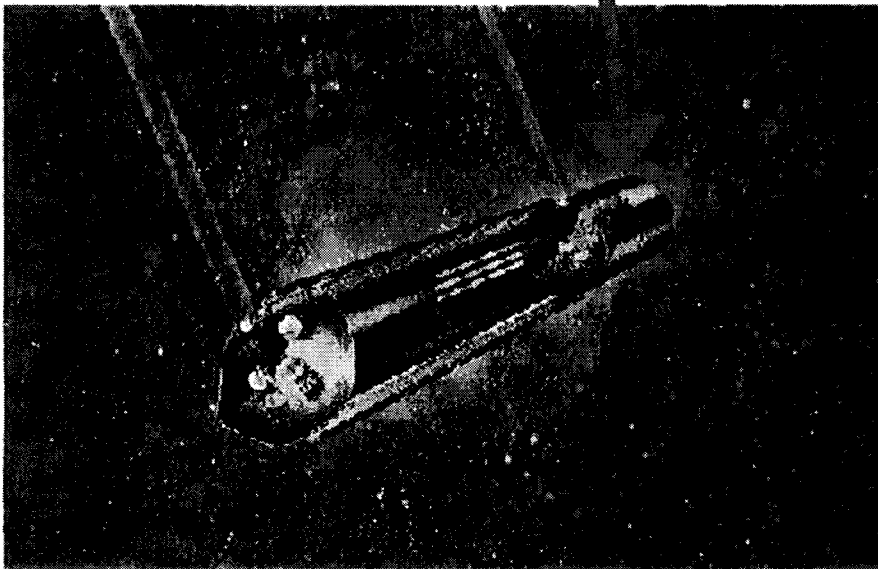
Pasadena, CA



JPL



NEW MILLENNIUM  
FORMATION FLYING  
INTERFEROMETER  
DEEP SPACE 3

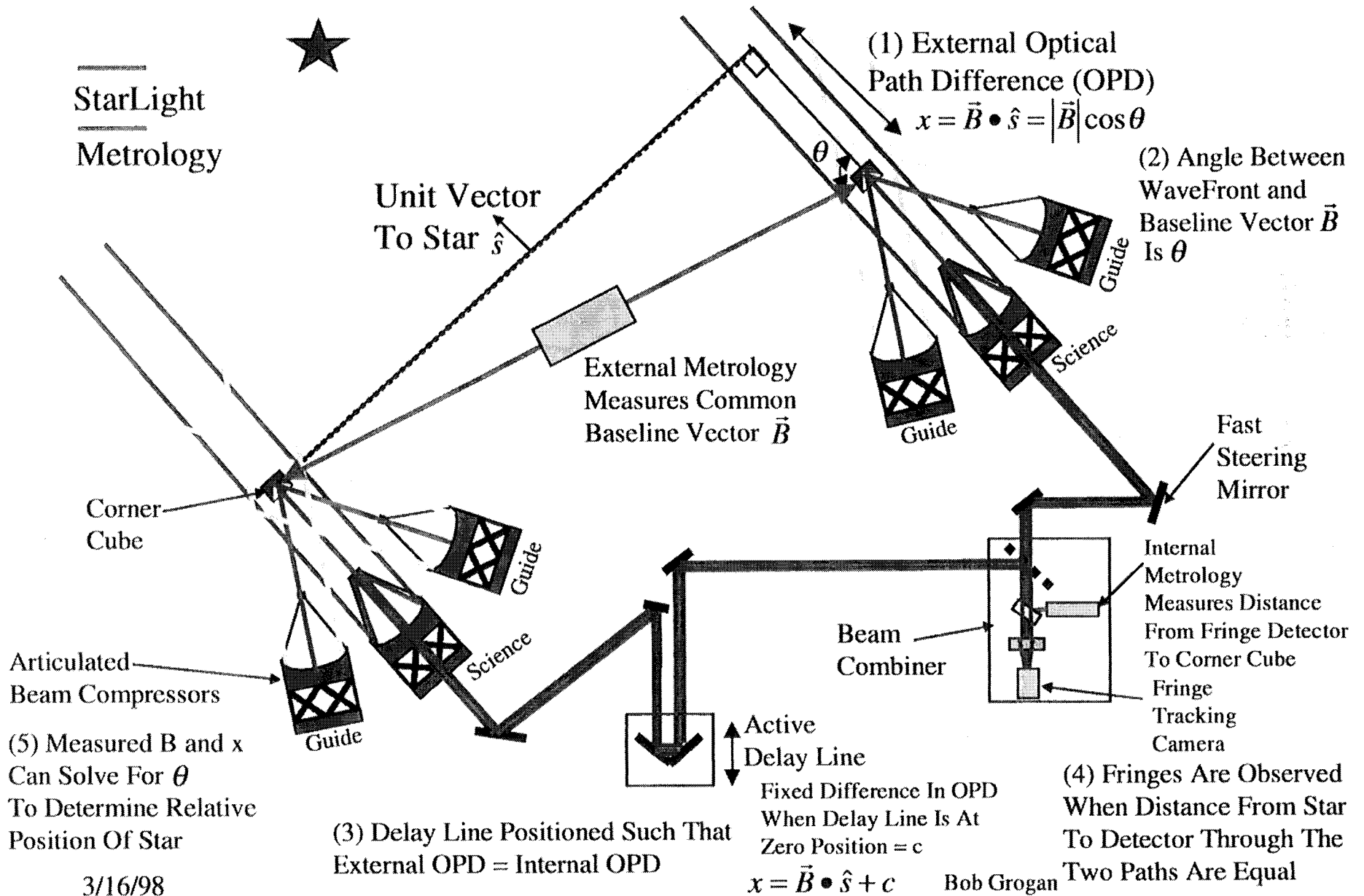


SPACE INTERFEROMETRY MISSION

3/16/98

Bob Grogan

# ROLE OF DELAY LINE IN INTERFEROMETER



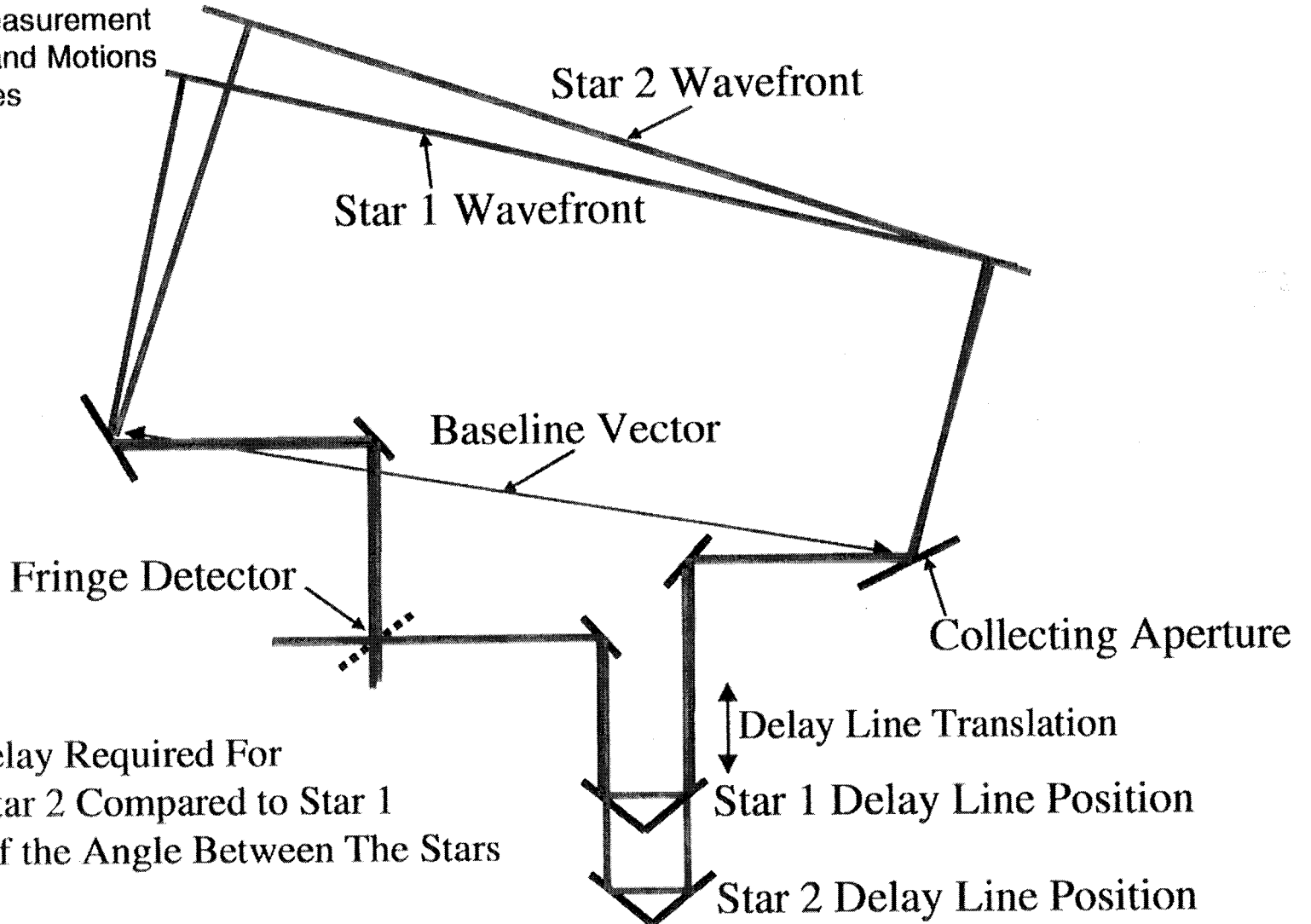


## ROLE OF DELAY LINE IN INTERFEROMETER

- Light From Star Arrives at One Telescope Sooner Than the Other Resulting In An External Optical Path Delay (OPD)
- $\theta$  Is The Angle Between Stellar Wavefront and Interferometer Baseline
- External OPD Is Determined by Introducing Internal OPD Which Exactly Matches It.  
Delay Line Positioned Such That External OPD = Internal OPD
- Fringes Are Observed When Distance From Star to Detector Through the Two Paths Are Equal. Feedback Is Used To Adjust Delay Line Position To Remain At The Peak of the Fringe.
- Baseline Vector ( $B$ ) Is Measured and  $X$  Is Determined From Delay Line Position. By Solving for  $\theta$  the Relative Position of the Star Is Determined

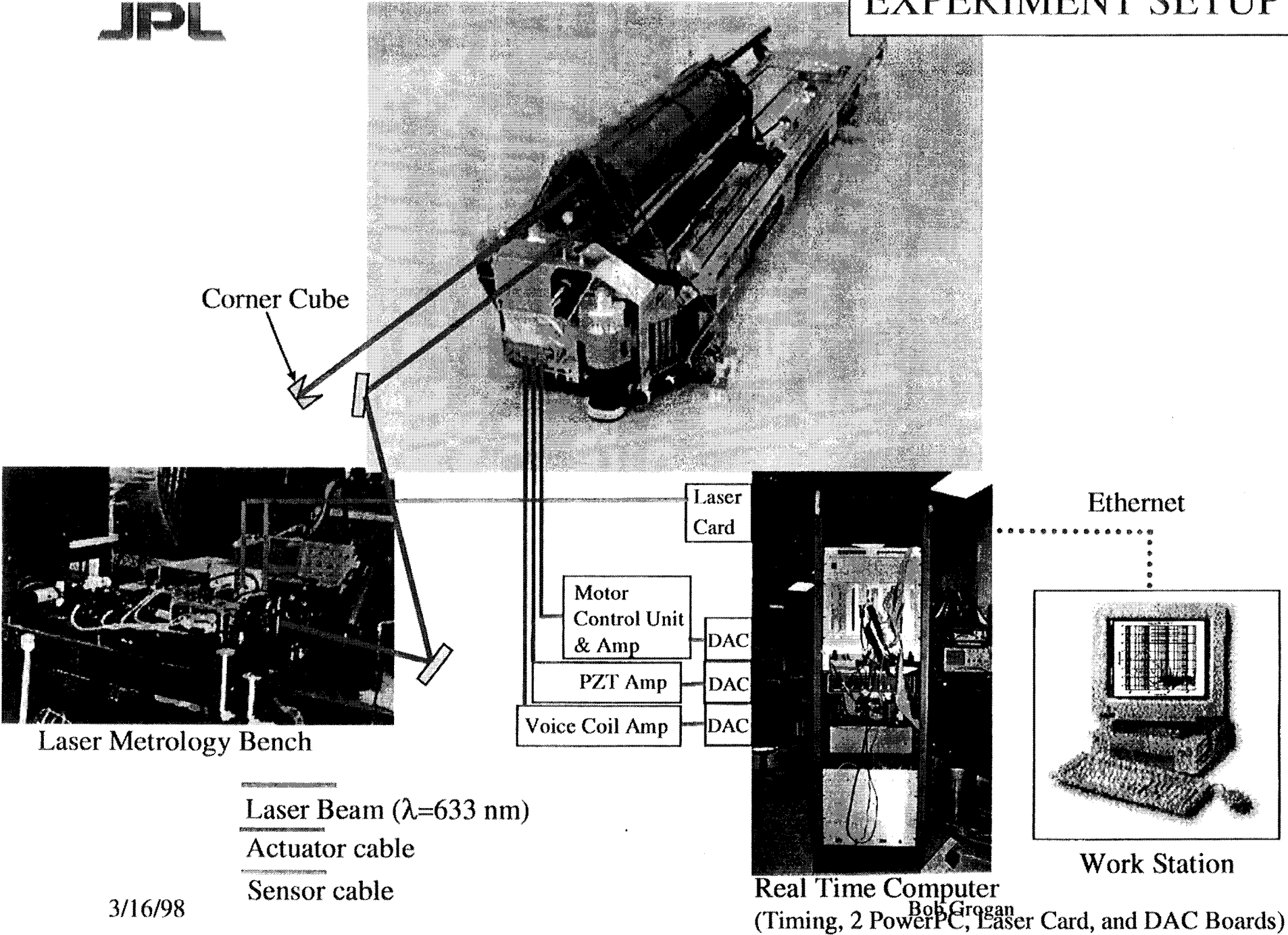
# ASTROMETRY

Astrometry  
The Scientific Measurement  
of the Positions and Motions  
of Celestial Bodies



Measured Delay Required For  
Fringes on Star 2 Compared to Star 1  
Is Measure of the Angle Between The Stars

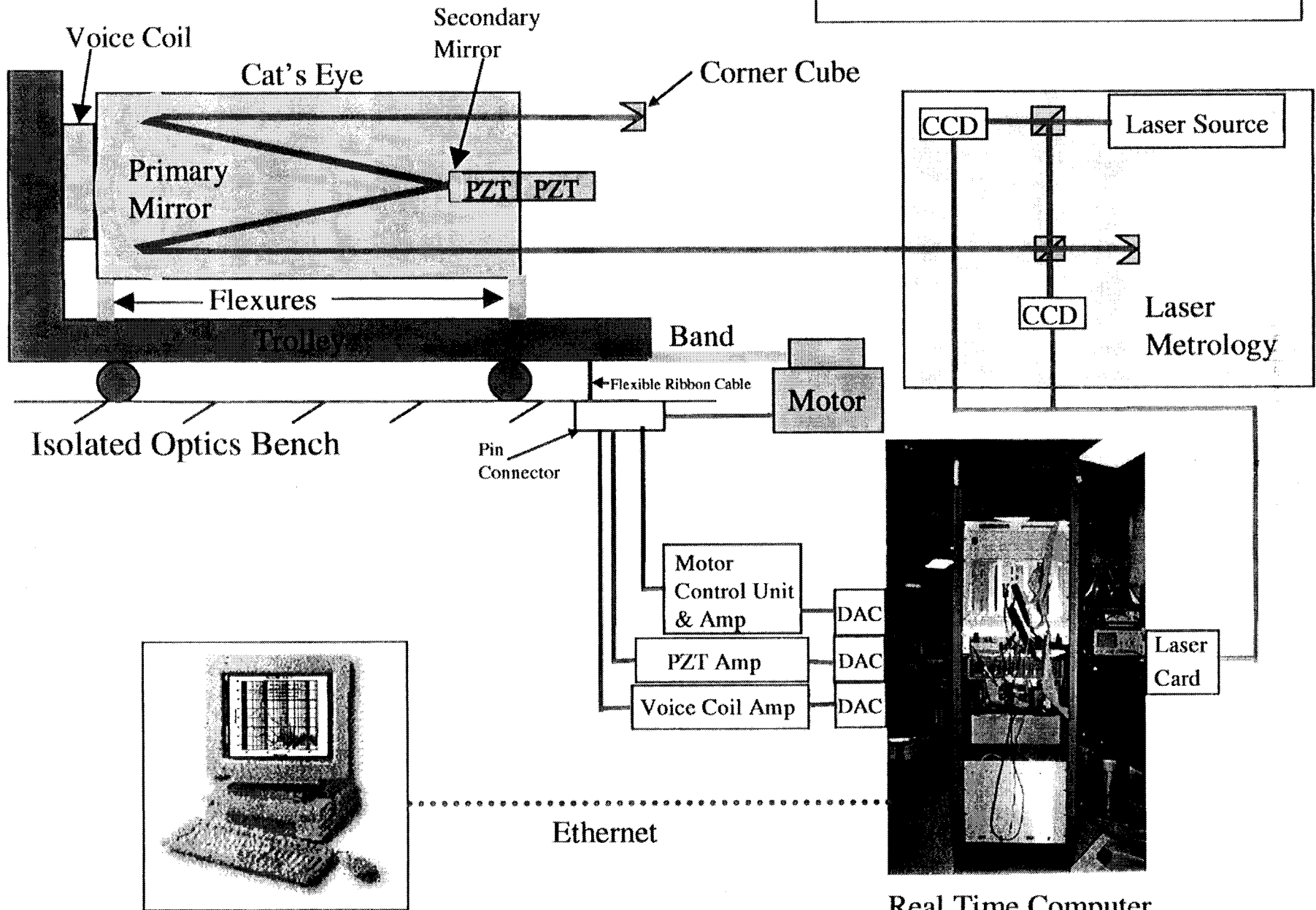
EXPERIMENT SETUP



3/16/98

JPL

EXPERIMENT SETUP



3/16/98

Work Station

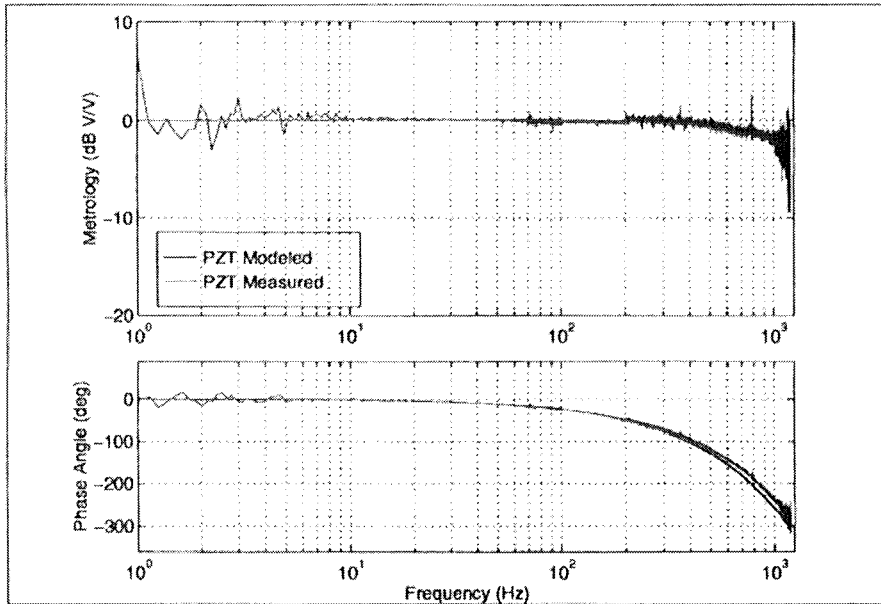
Real Time Computer  
Bob Grogan  
(Timing, 2 PowerPC, Laser Card, and DAC Boards)



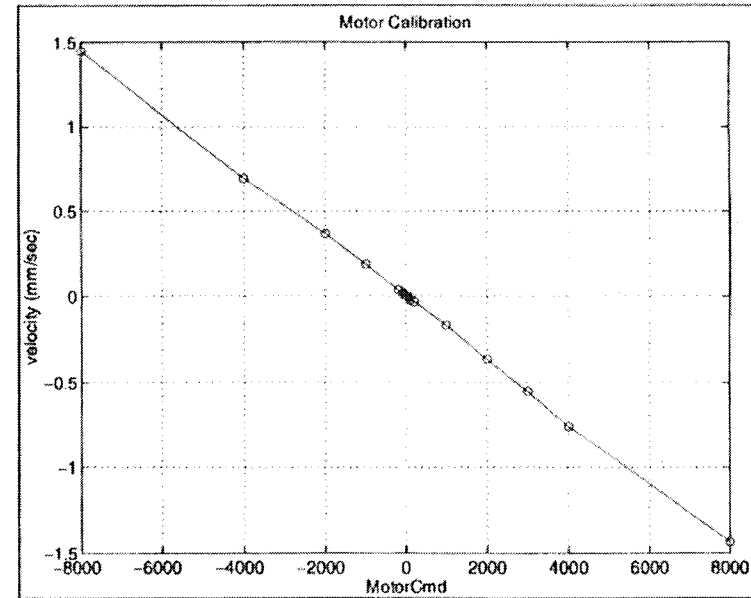
- Sensor
  - 1-D Measurement Along Light Path From Metrology Bench to Corner Cube
  - Wavelength = 633 nm
  - Laser Card
    - Digital Phase Meter Counts Phase Difference Between Reference and Unknown
  - 8 Bit Resolution
    - $633\text{nm}/(2*2^8) \Rightarrow 1.24 \text{ nm}$  Optical Jitter
  - Read at RTC Sample Rate  $\Rightarrow 5 \text{ kHz}$
  
- Actuators
  - PZT
    - Balanced PZT Stack for Reaction Compensation
    - DAC Command Resolution = 16 bits
    - PZT Integrator Card
    - Stroke 15 microns
    - PZT Loop  $\Rightarrow 5000 \text{ Hz}$
  - Voice Coil
    - Stroke = +/- 3 mm
    - DAC Command Resolution = 16 bits
    - Voice Coil Loop  $\Rightarrow 1000 \text{ Hz}$
  - Motor
    - DC Brushless Harmonic Drive
    - Band Drive
    - Command By Pulse Train Proportional to Encoder Lines/sec
    - Motor Loop  $\Rightarrow 100 \text{ Hz}$



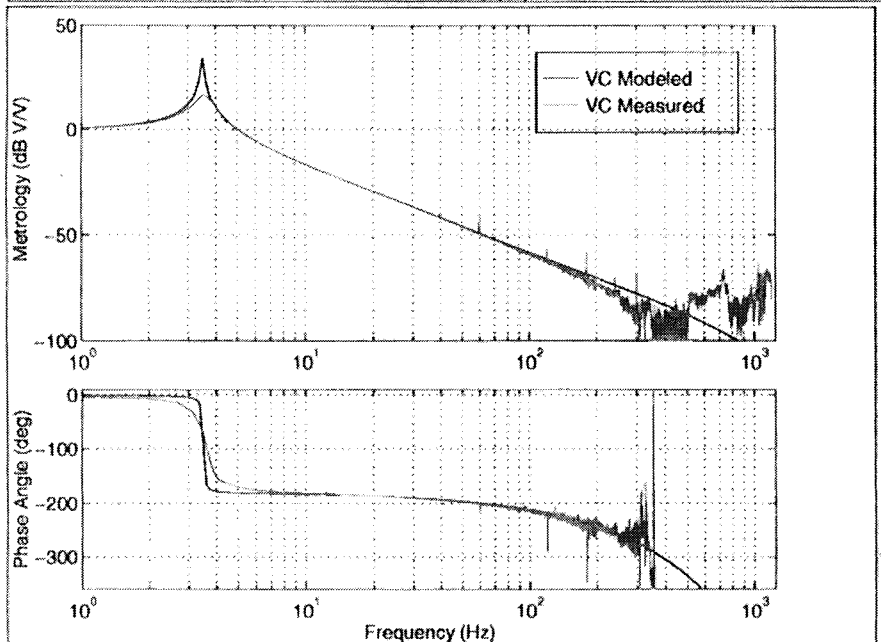
# PLANT CHARACTERIZATION



← PZT STAGE PLANT



MOTOR STAGE  
FEEDFORWARD  
CALIBRATION

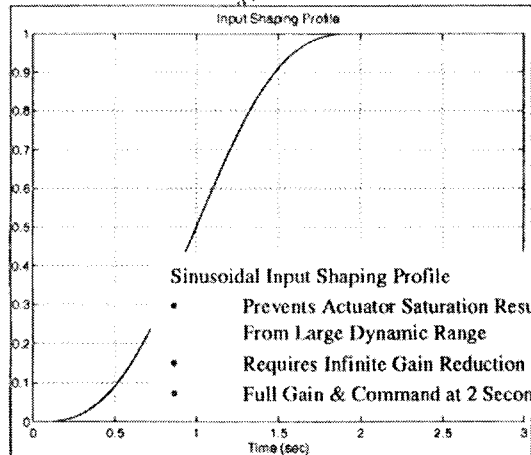
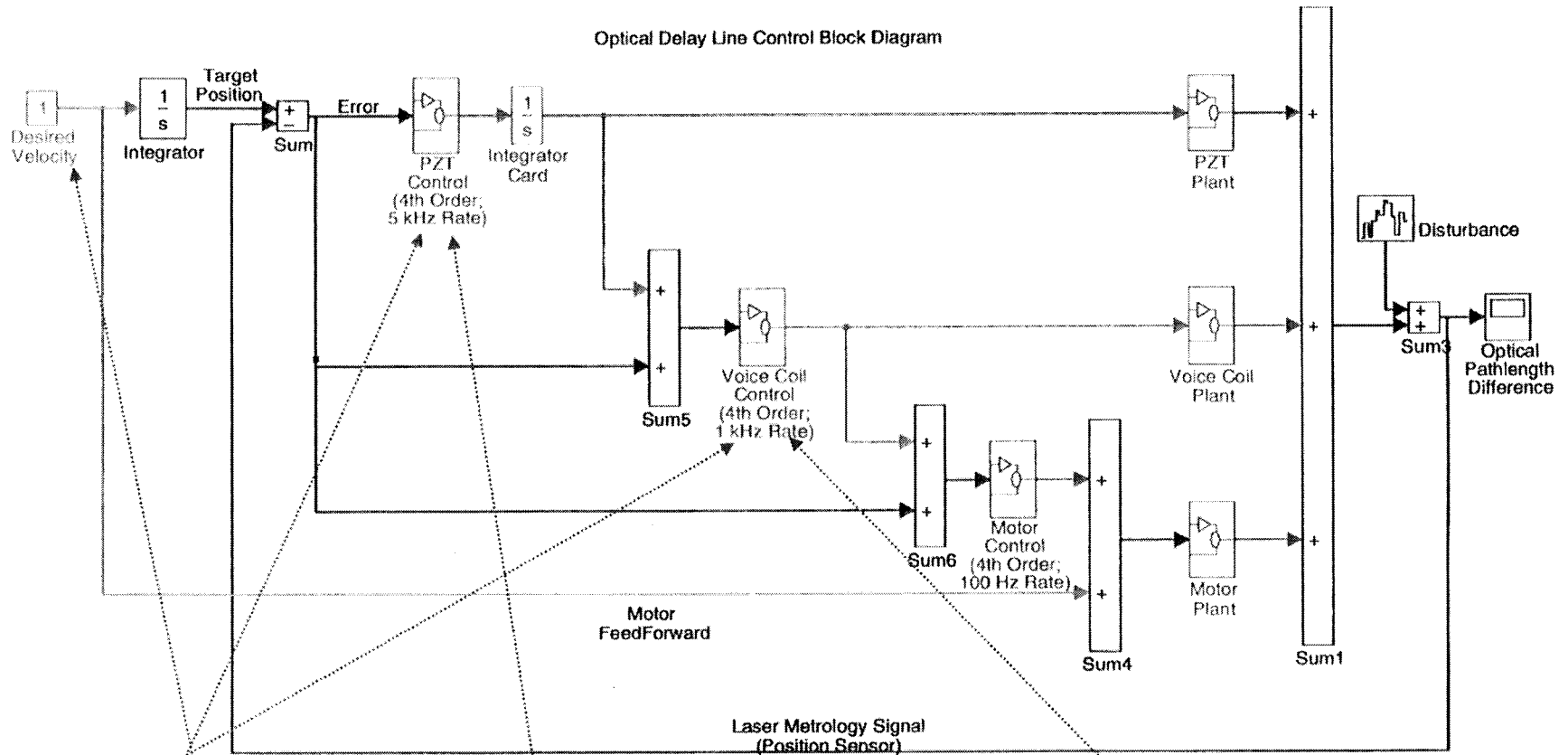


← VOICE COIL STAGE PLANT

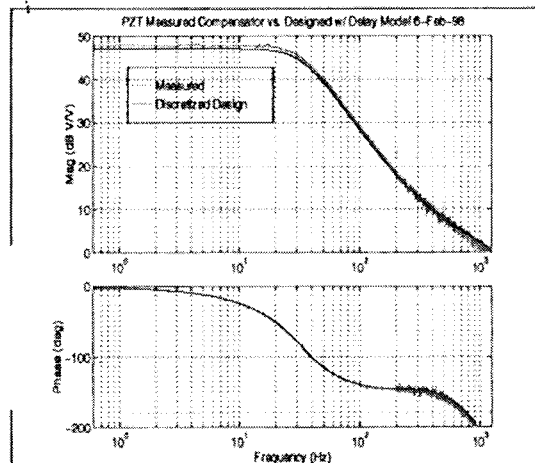
Bob Grogan

# CONTROL BLOCK DIAGRAM

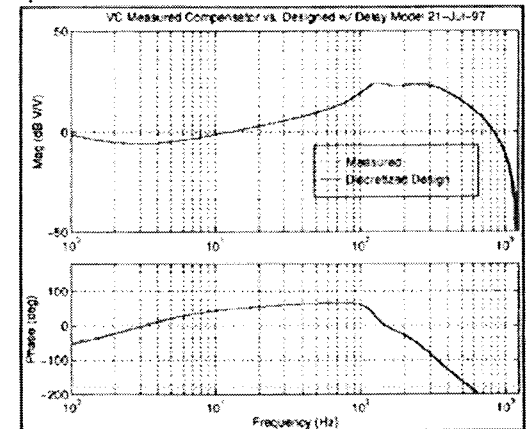
Optical Delay Line Control Block Diagram



3/16/98  
Input Shaping Profiles



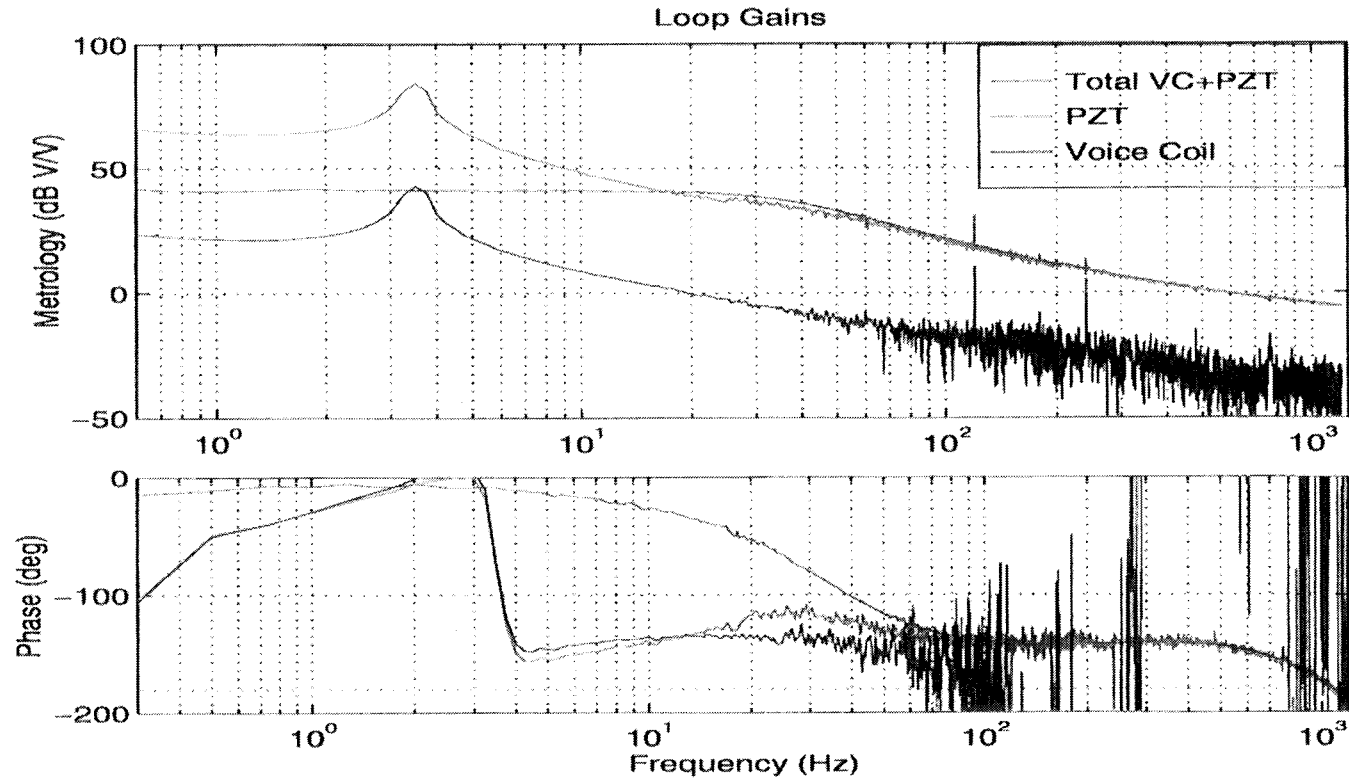
PZT Compensator



Bob Grogan  
Voice Coil Compensator



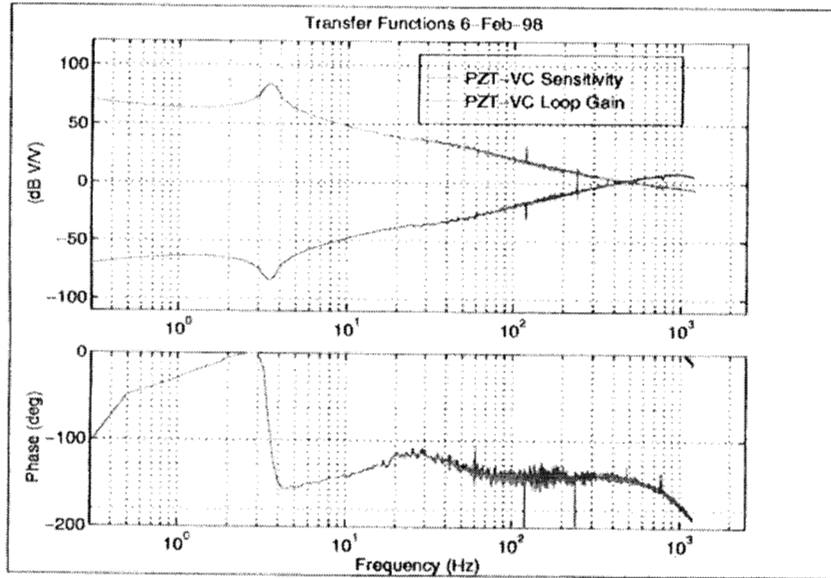
# CLASSICAL LOOP SHAPING DESIGN



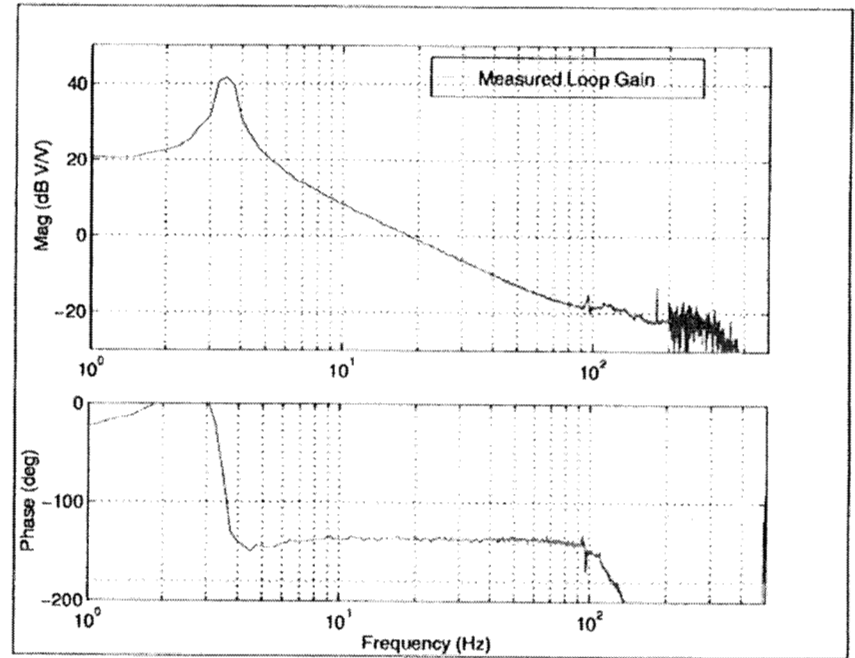
- Cascade Control Design
  - Coarse Stage Desaturates Fine Stage
  - Feedforward Velocity Command To Motor



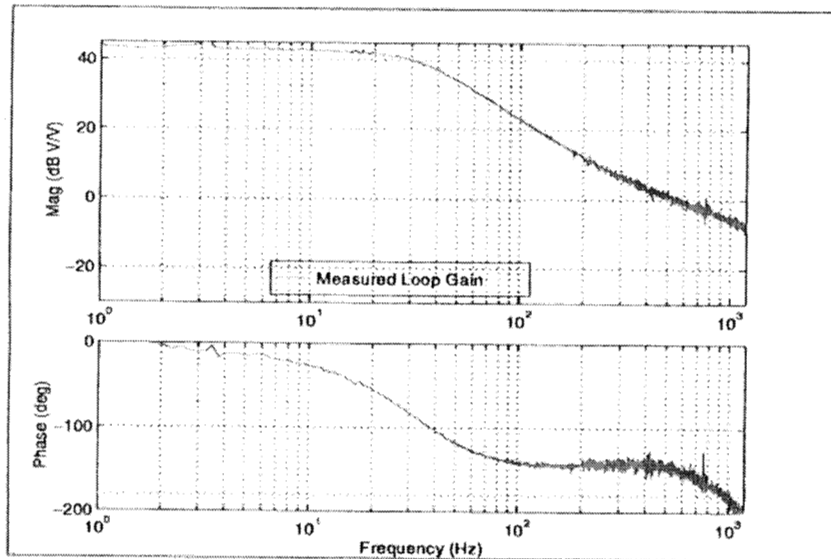
# LOOP GAINS



TOTAL LOOP GAIN and SENSITIVITY



VOICE COIL STAGE LOOP GAIN



3/1 PZT STAGE LOOP GAIN

## CONTROL ANALYSIS

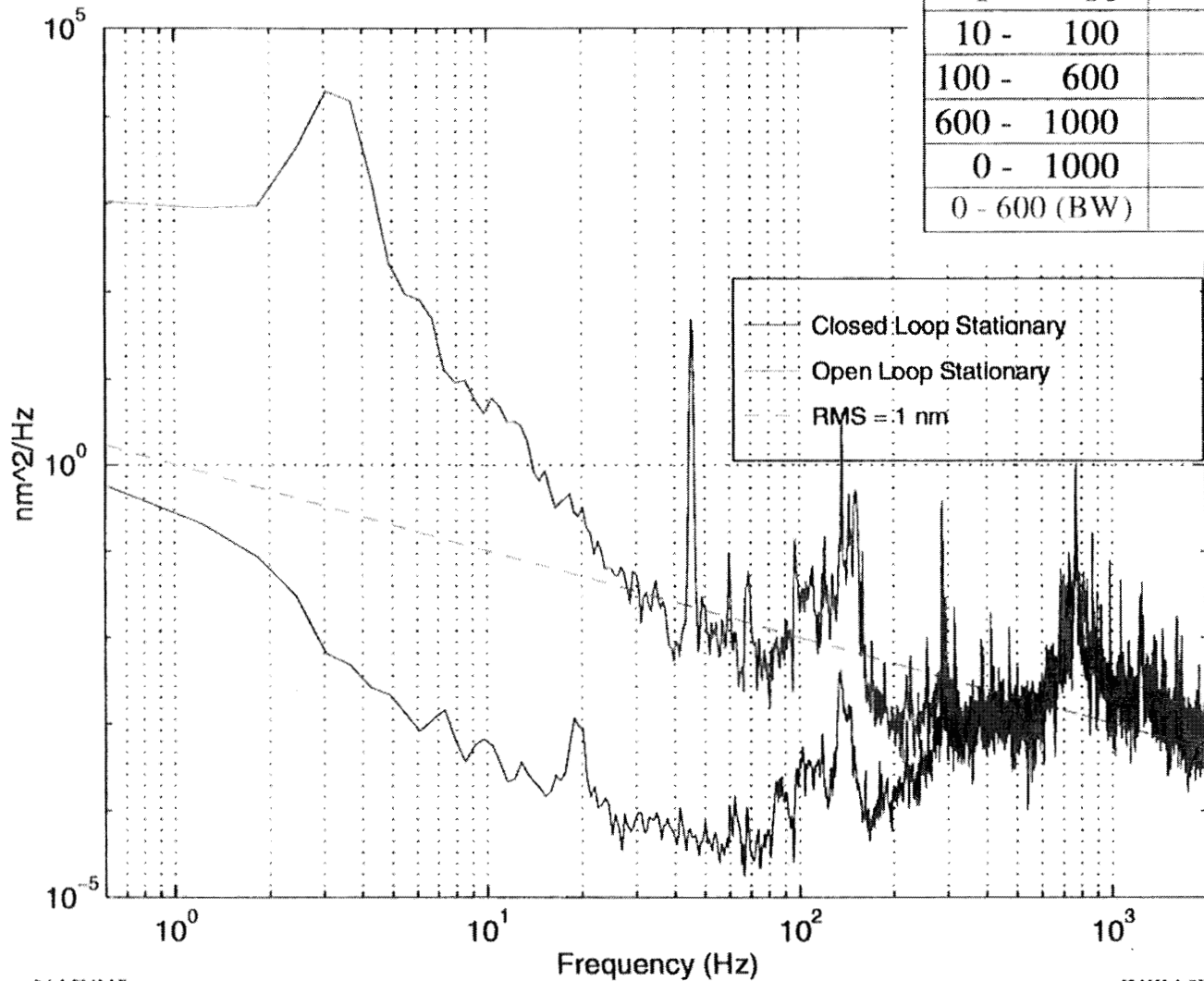
	Gain Margin (dB)	Phase Margin (deg)	Bandwidth (Hz)
Motor	50	100	0.1
Voice Coil	15	45	20
PZT	6	32	600
Total	6	32	600

Bob Grogan



# CLOSED LOOP PERFORMANCE OPTICAL JITTER STATIONARY CONDITION

Freq. Range (Hz)	RMS Jitter Open Loop Stationary (nm)	RMS Jitter Closed Loop Stationary (nm)
0 - 1	20.2	0.5
1 - 10	159.5	0.4
10 - 100	8.2	0.1
100 - 600	3.2	0.9
600 - 1000	3.3	2.3
0 - 1000	161.6	2.5
0 - 600 (BW)	161.5	1.0





# CLOSED LOOP PERFORMANCE

## OPTICAL JITTER 2 MM/SEC SLEW CONDITION

Freq. Range (Hz)	RMS Jitter Open Loop 2 mm/s (nm)	RMS Jitter Closed Loop 2 mm/s (nm)
0 - 1	4374	0.3
1 - 10	65826	2.6
10 - 100	107.2	1.4
100 - 600	4.8	1.6
600 - 1000	3.2	4.1
0 - 1000	66075	5.4
0 - 600 (BW)	66075	3.6

